Journal of Petroleum Science and Technology 14(1): 41, 2024, Pages 2-15
DOI:10.22078/jpst.2024.5406.1934

Journal of Petroleum Science and Technology

Research Paper

https://jpst.ripi.ir/

Interfacial Tension in Asphaltenic Crude Oil – Brine Systems: Robust Predictive Tools Based on Intelligent Approaches

Mohammad Amin Moradkhani and Seyedeh Hosna Talebian*

Department of Chemical and Petroleum Engineering, Faculty of Engineering, Ilam University, Ilam, Iran

Abstract

Accurate interfacial tension (IFT) determination between crude oil and brines is crucial in enhanced oil recovery (EOR) processes. However, the available IFT models only apply to systems containing pure hydrocarbons and saline waters. The current study aims to design comprehensive predictive tools for the IFT between asphaltenic crude oils and various brines. Hence, 339 relevant experimental data covering an extensive range of operating conditions were gathered from the literature, and the most effective input variables were determined through Spearman's rank coefficient. Then, the experimental data were utilized to train the smart soft-computing approaches, i.e., radial basis function (RBF), multilayer perceptron (MLP), and Gaussian process regression (GPR). Although all novel predictive tools presented excellent results, the one designed based on the GPR method was recognized as the most reliable model with an average absolute relative error (AARE) of 0.67% and an *R2 value of 99.63%* in the testing stage. Additionally, it estimated most of the IFT data with relative errors below 0.10%. On the other hand, the validity of the gathered databank was confirmed through the leverage method. The influences of pressure, temperature, salinity, and structural characteristics of salts on the IFT were discussed in detail, and the proposed models favorably described the physical trends. Eventually, a sensitivity analysis was carried out based on the GPR model to clarify the order of significance of factors in controlling the crude oil-brine IFT.

Keywords: Interfacial Tension; Asphaltenic Crude Oil; Brine; Intelligent Approaches; Modeling.

Introduction

Interfacial tension (IFT) is a fundamental factor that describes the behavior of molecules at the boundary of immiscible fluids [1–3]. The forces exerted on the molecules located in the bulk of fluids, and those at the interface are quite different, as shown in Fig. 1. The bulk molecules (A and B) receive equal attraction forces in all directions since similar molecules have surrounded them. Meanwhile, the interfacial molecules (such as C) are affected by unequal interactions from each side of the interface. This stems from the fact that the physical and chemical properties of the adjacent phases are quite different, and each of them may exert an independent force on the contact area [4]. Accordingly, the total force applied to the interfacial molecules is not zero. This difference in the applied forces, which causes a curvature in the interfacial area, is well-known as IFT [5–7].

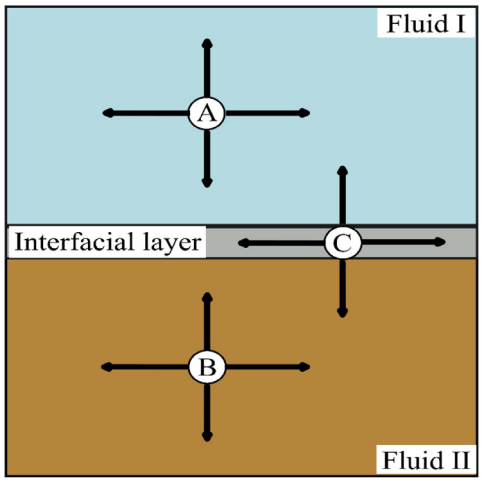

Fig. 1 Comparison between the forces exerted on molecules in two immiscible fluids.

**Corresponding author:* Hosna Talebian, Department of Chemical and Petroleum Engineering, Faculty of Engineering, Ilam University, Ilam, Iran
E-mail addresses: h.talebian@ilam.ac.ir
Received 2024-05-11, Received in revised form 2024-07-09 22, Accepted 2024-08-14, Available online 2024-10-21

Determining the IFT of oil-containing systems is particularly important in the petroleum industries [8–19]. Based on various investigations, the percentage of original oil recovered after the primary and secondary steps of the oil recovery process mainly varies between 20-30% [20,21]. The oil ganglia are entrapped by the throats and pores' capillary forces and remain unrecovered during the process. Consequently, it is essential to implement the enhanced oil recovery (EOR) processes to reduce the capillary forces and recover as much oil as possible from the reservoir [22–31]. The impact of capillary forces on the oil reservoir is usually described by a dimensionless factor called capillary number [32],

$$Ca = \frac{Viscose\ forces}{Capillary\ forces} = \frac{U\mu}{\gamma\cos(\theta)} \quad (1)$$

where the symbols U, μ, θ, and γ stand for the velocity, viscosity, contact angle, and IFT [33]. The foregoing equation indicates that the reduction of IFT through the EOR techniques can be recognized as an efficient way to enhance the capillary number and improve the oil recovery [34, 35]. The saline water injection is a well-known EOR method through which the mobility of trapped oil is boosted due to the IFT reduction [36–38]. Accordingly, investigating the IFT of crude oil-brine systems under various operating conditions can contribute to the optimal design of the EOR process [39]. Several experimental studies reported the IFT of oil–brine blends [16,40]. In most of these studies, pure alkanes have been considered the oil phase, and investigations on the IFT of crude oil-brine are limited. Lashkarbolooki et al. [41] studied the impact of various monovalent and divalent salts on the IFT of asphaltenic crude oil with a specific gravity of 0.9224.

The results demonstrated that the best performance in reducing the IFT can be attributed to the divalent cations blended with the chloride ion. Additionally, it was found that the monovalent salts have insignificant effects on the IFT since they have low synergy with the natural surfactants present in the crude oil. Moeini et al. [42] experiments revealed that the IFT of dead oil-brine is reduced with an increase in brine concentration up to 30,000 ppm. After that, an exponential increase was observed in the IFT by enhancing salinity. In another work, Barati-Harooni et al. [4] measured the IFT of live oil-brine blends over extensive brine salinity, pressure, and temperature ranges. This study, in which two oil samples with quite different amounts of asphaltene were analyzed, indicated that brine salinity and pressure directly correlate with IFT. However, the relationship between IFT and pressure was contradictory in the oil samples. While the IFT of the sample with low asphaltene content was reduced with increasing temperature, the other sample experienced considerable growth in IFT due to the foregoing change. Moreover, the effects of pressure and salinity on the IFT of asphaltenic crude oil – NaCl has been assessed by Soleymanzadeh et al. [43]. The major findings of this study were the linear increasing trends of IFT versus brine concentration and pressure. Considering the structural ability of asphaltene compounds to accumulate at the interface between water and oil and act as a surface-active material and the uncertainties surrounding its influence on IFT, it is necessary to evaluate the IFT of asphaltenic oil-brine systems [44]. The precipitation and subsequent deposition of asphaltene in the reservoir can result in the rock's wettability becoming strongly oil-wet, affecting the relative permeabilities and oil recovery [20,45,46].

Since determining the IFT of various systems through experimental measurements is costly and time-consuming, data-driven approaches have recently been widely implemented to derive predictive models for this critical factor [1,8,22,24,47–60]. In the case of oil–brine systems, existing studies have mainly focused on synthetic oils as the hydrocarbon phase. Amar et al. [48] designed four intelligent models for the IFT of hydrocarbon–brine systems based on 560 measured data. The high capability of intelligent methods to describe the IFT was demonstrated since the AARE values of the proposed models varied between 1.06% and 2.06% in the testing step. Abooali et al. also employed the same database [61] to establish a mathematical correlation for the IFT based on the genetic programming method. The outcomes of the suggested correlation were in proper consistency with experimental data, with a total AARE of 3.89%. The only predictive tool for the IFT of crude oil-brine was presented by Barati-Harooni et al. [4], who utilized their experimental data to derive an intelligent model based on the least square support vector machine (LSSVM) approach. The proposed model correlated the IFT with pressure, temperature, and concentration of NaCl. Despite giving an AARE of 1.12% for testing data, this model could not describe the influences of oil characteristics and brine type on the IFT.

According to the literature review above, most existing models estimate the IFT of pure hydrocarbon–brine systems. The optimal design of the EOR process requires accurate knowledge regarding the reservoir crude oil-brine IFT [62]. On the other hand, smart modeling approaches have not yet been used to derive comprehensive and well-validated predictive tools for this fundamental parameter. Furthermore, identifying the most effective factors on the IFT of crude oil-brine system behavior is particularly important for field development planning.

To fulfill the mentioned research gaps, in the current study, an immense set of data, including 339 experimental samples pertinent to the IFT of various asphaltenic crude oil-brine systems over a broad range of operating conditions, were gathered from the literature. The intelligent modeling phase uses three well-known soft-computing methods: MLP, RBF, and GPR. A set of statistical and visual criteria was used to assess the validity and reliability of the proposed model, and the variations of IFT with operational parameters were studied based on the outcomes of the models. Eventually, the order of importance of factors in controlling the IFT of crude oil-brine systems is determined based on a sensitivity analysis.

Materials and Methods

Smart Approaches

GPR

The application of non-parametric machine learning approaches such as GPR, a Gaussian joint probability distribution, has increased widely in engineering in recent years due to their high robustness and capabilities [63]. The main preponderances of GPR are high accuracy and strength

in modulating the hyper-parameters and the ability to catch the uncertainty of analyzed samples.

The GPR-based learning process is accomplished through a probabilistic framework in which a training dataset $T=[(x_i,y_i) \quad i=1,2,...,n]$ is provided. It should be noted that x_i and yi stand for the input variables vector and target function, respectively. Thus, the predictive model provides the output function distribution at any point through the following approximation [64],

$$y_i = g(x_i) + \varepsilon_i \tag{2}$$

where $L(x_i)$ is the latent function corresponding to the input variables (x_i), and its values constitute a random variable. Furthermore, ε_i represents the Gaussian noise, with its mean and variance presented as 0 and σ_n^2, respectively [65],

$$\varepsilon_i=N(0,\sigma_n^2) \tag{3}$$

Consequently, the target function can be easily approximated by defining a mean function $m(x)$ and a covariance function cov(x,x'). The predictive probability distribution for the input variables, x^* can be defined as,

$$\hat{y}^* = m(x^*) + k_*^T (K+\sigma_n^2 I)^{-1}(y - m(x^*)) \tag{4}$$

$$\sigma_{y^*}^2 = k_* + \sigma_n^2 - k_*^T (K+\sigma_n^2 I)^{-1} k_* \tag{5}$$

where k^* is defined as $[k^*]_i=\text{cov}(x_i,x^*)$, K stands for a covariance matrix, and its elements are $[K](i,j)=\text{cov}(x_i,x_j)$, and I shows the identity matrix.

As the predictive probability distribution is specified by the hyperparameters, an optimization process should be carried out to determine these factors [66]. In the GPR approach, the log-likelihood function is maximized during the training stage to calculate the hyperparameters [67],

$$\log p(y \mid X) = -\frac{1}{2} y^T (K+\sigma_n^2 I)^{-1} y - \frac{1}{2}\log(|(K+\sigma_n^2 I)|) - \frac{\pi}{2}\log(2\pi) \tag{6}$$

where n represents the number of training data points.

MLP

The MLP machine learning approach follows a similar process to that observed in the human nervous system and is mainly implemented to solve complicated mathematical problems, such as approximation, classification, and pattern recognition [68]. This is performed through a parallel algorithm, in which a set of data is utilized to train the network, and the artificial neurons are responsible for transferring the information. Fig. 2 shows the structure of an artificial neuron employed in the MLP network. The neuron is mathematically explained as follows [69],

$$r_a = \sum_{i=1}^{n} x_i W_{ai} + b_a \tag{7}$$

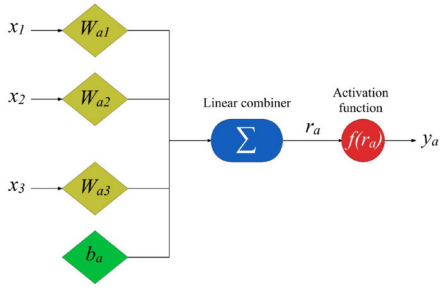

Fig. 2 Details of an artificial neuron.

$$y_a = f(r_a) \tag{8}$$

Where r_a, x_i, W_{ai}, b_a and y_a stand for linear combiner, i th input factor, synaptic weight, neuron bias, and activation function, respectively.

As the MLP processes the information only in one direction, it is recognized as a feed-forward network. The graphical description of the MLP network designed to model the crude oil-brine IFT is illustrated in Figure 3, which shows three linked layers, including artificial neurons. The input, hidden, and output layers are responsible for introducing the information to the network, determining the network parameters, and displaying the outcomes, respectively. It should be highlighted that the architecture of the hidden layer depends on the complexity of the problems, and may contain some independent layers with different numbers of neurons in each of them, while the number of neurons in the first and last layers is equal to the number of input and output variables, respectively. The MLP network detects the system's nonlinearity via the activation functions included in the hidden layer's neurons [70]. In the current study, after assaying various architectures, a network with two hidden layers containing 12 neurons, each accounts for the best precision for estimating the crude oil-brine IFT. The tan-sigmoid function was adjusted in the neurons as an activation function.

A vital stage in designing the MLP network, which considerably affects the capability of the network, is the optimization of weights and biases. For this purpose, the backpropagation (BP) algorithm specifies the foregoing parameters, so that the minimum value of the deviation function is obtained [71],

After applying each training data, the value of the deviation function is spread in the network, followed by re-adjusting the parameters. Herein, the Bayesian regularization approach was used to train the BP algorithm.

$$D = (y_{pre} - y_{\exp})^2 \tag{9}$$

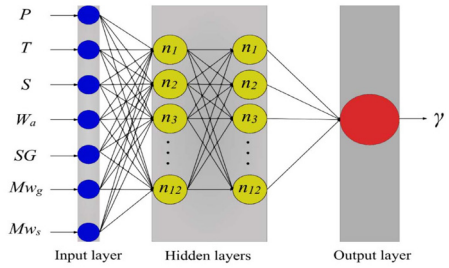

Fig. 3 The structure of the MLP network is employed to estimate the crude oil-brine IFT.

RBF

RBF networks were developed mainly to mitigate the drawbacks of MLP networks, such as their empirical structure and under or over-fitting possibility. The high potency for interpolation, prompt convergence, simple structure, and sublime reliability are the main advantages of RBF networks [72]. The structure of this network is similar to that of a single-layer MLP network, which includes several neurons equal to the number of data points used for training. Furthermore, the structure of the RBF network employed to model the crude oil-brine IFT is demonstrated in Fig. 4.

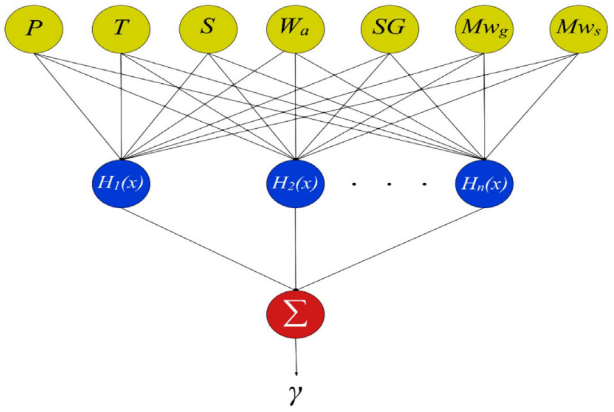

Fig. 4 The structure of the RBF network employed to estimate the crude oil – brine IFT.

It should be noted that the activation functions employed in these networks are radial-based, among which the most well-known function is Gaussian,

$$H(x)=\exp(-\frac{(x-c)^2}{r^2}) \quad (10)$$

where c and r are the center and radius of the Gaussian function, respectively.

After receiving the information from the input layer, the hidden layer exerts the nonlinear functions and sends the results to the final layer, which is responsible for combining the weights and the activation functions, linearly [73],

$$f(x)=\sum_{i=1}^{n} W_i H_i(x) \quad (11)$$

The gradient descent method is employed in the RBF network to optimize the network center and synaptic weights so that the mean squared error (MSE) is minimized,

$$\mathrm{MSE}=\frac{1}{n}\sum_{i=1}(y_{pre}-y_{exp}) \quad (12)$$

Experimental Data Acquisition

Since the capability of the predictive tools strongly depends on the databank used for designing them, gathering the maximum number of reliable data concerning the IFT of crude oil-brine systems built the main cornerstone of the present research. Moreover, the operating conditions of the analyzed sources are reported in Table 1. The databank includes 339 experimental samples pertinent to the IFT of asphaltenic live and dead oils blended with various saline waters over a broad range of pressures and temperatures. Additionally, the asphaltene content of the data sources analyzed is in a range of 3.1 to 13.75%, which is the asphaltene content associated with medium to light crude oil systems of conventional oil reservoirs [74]. Thereupon, the present databank can be employed to derive robust and comprehensive predictive tools.

Error analysis

The accuracy of the predictive tools proposed in this study is evaluated by calculating the values of the following statistical parameters,

$$AARE\ (\%)=\frac{\sum|E_i|}{N}\times 100 \quad (13)$$

$$SD\ (\%)=\sqrt{\frac{\sum(E_i-\bar{E}_i)^2}{N-1}}\times 100 \quad (14)$$

$$SD\ (\%)=\sqrt{\frac{\sum(E_i-\bar{E}_i)^2}{N-1}}\times 100 \quad (15)$$

$$R^2\ (\%)=(1-\frac{\sum(y_{pre}-y_{exp})^2}{\sum(y_{exp}-\bar{y}_{exp})^2})\times 100 \quad (16)$$

where E_i stands for the relative error of ith estimated data,

$$E_i=\frac{y_{pre,i}-y_{exp,i}}{y_{exp,i}} \quad (17)$$

Results and discussions

Determining the input variables of the models

According to experimental investigations, the IFT of crude oil–brine systems is dependent not only on pressure, temperature, and salinity, but also on the characteristics of crude oil and salts. In this study, the influences of oil properties on the IFT were taken into account by defining the specific gravity as well as the percentage of asphaltene as input variables. On the other hand, the molecular weight of salts was considered as an adjusted parameter to make the models applicable to various types of saline water. Additionally, for distinguishing between live and dead oils, the equivalent molecular weight of dissolved gases was also included among the input factors,

$$Mw_g=\frac{1}{\sum_{i=1}^{n}\frac{W_i}{Mw_i}} \quad (18)$$

Table 1 Operating conditions of the data sources analyzed in this study.

Source	Crude oil	SG	Asphaltenes composition, (%)	Salt comp.	Salinity (ppm)	Temperature, (K)	Pressure (psia)	No.
[4]	Live oil	0.854, 0.915	3.18, 11.41	NaCl	0 to 260,000	298.15 to 383.15	2500 to 4500	240
[43]	Dead oil	0.9224	11	NaCl, KCl, $CaCl_2$, $CaSO_4$, $MgCl_2$, $MgSO_4$, Na_2SO_4	0 to 45,000	313.15	14.7	33
[42]	Live oil	0.933	13.75	NaCl, $CaCl_2$	5000 to 200,000	313.15	14.7 to 2500	36
[43]	Live oil	0.814	3.1	NaCl	50,000 to 260,000	298.15	2500 to 4500	30
Total	Live and dead oil	0.814 to	3.1 to 13.75	7 Different salts	0 to 260,000	298.15 to 383.15	14.7 to 4500	339

It should be noted that the value of Mw_{dg} is zero for dead oils. As a result, the relationship between the input and output variables can be expressed as follows,

$$y = f(P, T, S, W_a, SG, Mw_g, Mw_s) \quad (19)$$

Fig. 5 depicts a heatmap corresponding to the absolute values of Spearman's rank coefficient between the crude oil–brine IFT and the chosen input variables based on the analyzed data. The maximum correlation [75] between two given variables is achieved when the value of the foregoing coefficient tends to unity. According to the figure, all selected factors have noticeable impacts on IFT, and they must be taken into account in the models. It is interesting to note that the highest and lowest relationship with IFT can be attributed to S and W_a, respectively.

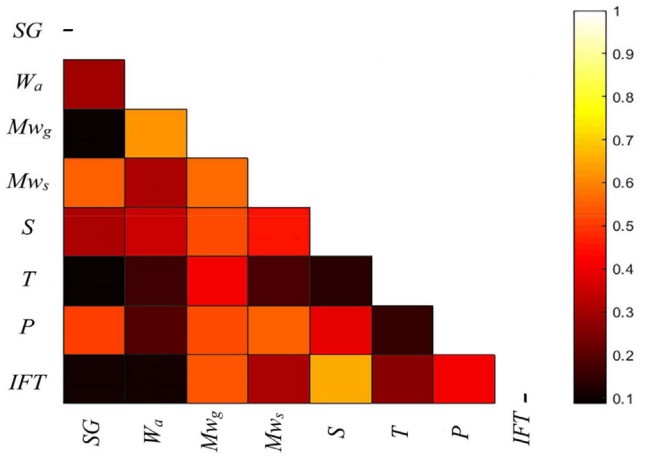

Fig. 5 Spearman's rank coefficient heatmap for input variables and the crude oil – brine IFT.

Development of the IFT Models Based on Smart Approaches

According to the form presented in Eq. (19), the collected databank was employed to design new predictive tools for the IFT of crude oil-brine systems based on the smart soft-computing methods of MLP, RBF, and GPR. It is worth noting that two different subsets, with an 80%-20% split ratio, were created by the collected data. The models were first trained based on the larger dataset (including 271 measured samples) and then tested using the remaining set of data (including 68 data points). It is worth mentioning that both the training and testing data points were selected randomly. The values of the statistical parameters pertinent to the smart models in the training and testing stages have been sketched in Fig. 6. A glance at the figure reveals that all smart approaches have almost identical and excellent performance during the training step with AARE values below 0.1%. However, their deviations in predicting the test dataset are associated with some differences. The highest level of precision belongs to the model designed by the GPR approach with AARE, RRMSE, SD, and R2 of 0.67%, 0.98%, 1.01%, and 99.63%, respectively. Since the accuracy and reliability of data-driven models are usually determined by their performance in the testing step, the foregoing values acknowledge the superiority of the GPR method from the mentioned points of view. Afterward, the RBF-based predictive tool is ranked second in terms of precision, since its AARE and R^2 values for the test dataset are 1.29%, and 98.77%, respectively. Ultimately, with the AARE of 1.45%, the MLP models can also be considered a reliable model to estimate the IFT of crude oil-brine systems. Interestingly, the proposed intelligent models are recognized as predictive tools with excellent capability according to the classification presented by Zendehboudi et al. [76] since all of them have RRMSE values far below 10%. This means that the input variables presented in Eq. (19) have been properly chosen, and the effects of various factors on the crude oil-brine IFT have been satisfactorily addressed in the novel models.

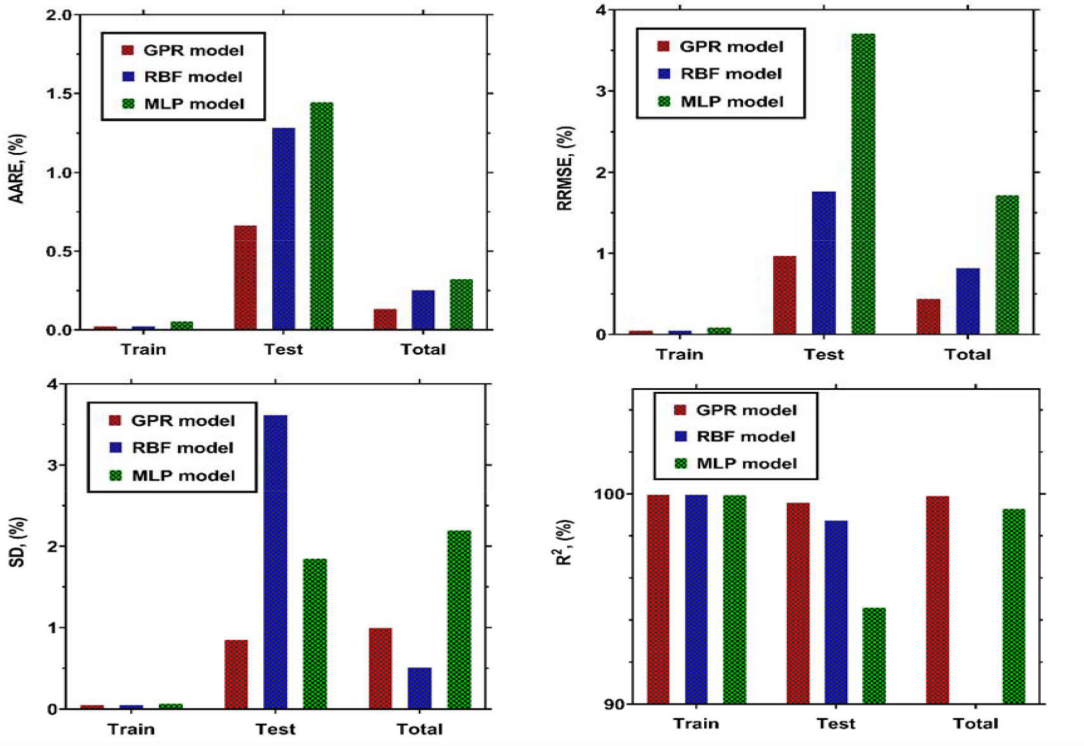

Fig. 6 The statistical error metrics obtained by the novel smart models for predicting the IFT of crude oil-brine systems.

Graphical description of the reliability of the novel models

Besides the pre-mentioned quantitative analyses, this section addresses a qualitative investigation of the reliability of the proposed smart paradigms by utilizing a set of visual representations, including a cross plot, cumulative frequency analysis, and contour diagram.

The cross plot of Fig. 7 compares the IFT values predicted by the smart methods with the corresponding measured data points. Allocating the values estimated by the models in the vicinity of the diagonal line is the criterion to judge the accuracy of each model. The outcomes of all predictive tools in the training phase are situated near the foregoing line, and no significant distances are observed between the line and the estimated points. However, the predictions of the GPR model for the testing dataset have better consistencies with the real data. While some deviations are seen between the values predicted by the remaining models and the best-fit line. Consequently, the GPR model can be regarded as the most precise predictive tool for the crude oil–based IFT. Moreover, the experimental databank analyzed in the current research, the computer program of the GPR model, and instructions on how to use the foregoing program to estimate the IFT have been included in the supplementary material. A comparison between the cumulative frequency [69] of the developed smart models has been presented in Fig. 8. This approach represents the percentage of data estimated within a certain level of relative deviation. Hence, an accurate model is expected to experience a sharp ascending trend at the beginning of its cumulative frequency curve. It is observed that most calculations carried out by the GPR, RBF, and MLP models are associated with relative errors below 0.1%, implying the fact that the aforementioned predictive methods have excellent performances in predicting the crude oil-brine IFT. Notwithstanding, the most favorable consistencies between calculated and actual data can be observed in the case of the GPR computational approach, which estimates 82.60%, 91.44%, 94.99%, 98.23%, and 99.71% of data with relative deviations less than 0.1%, 0.5%, 1%, 1.5%, and 2%, respectively. Consequently, the current evaluation provides another evidence concerning the superiority of the GPR predictive tool over the other models.

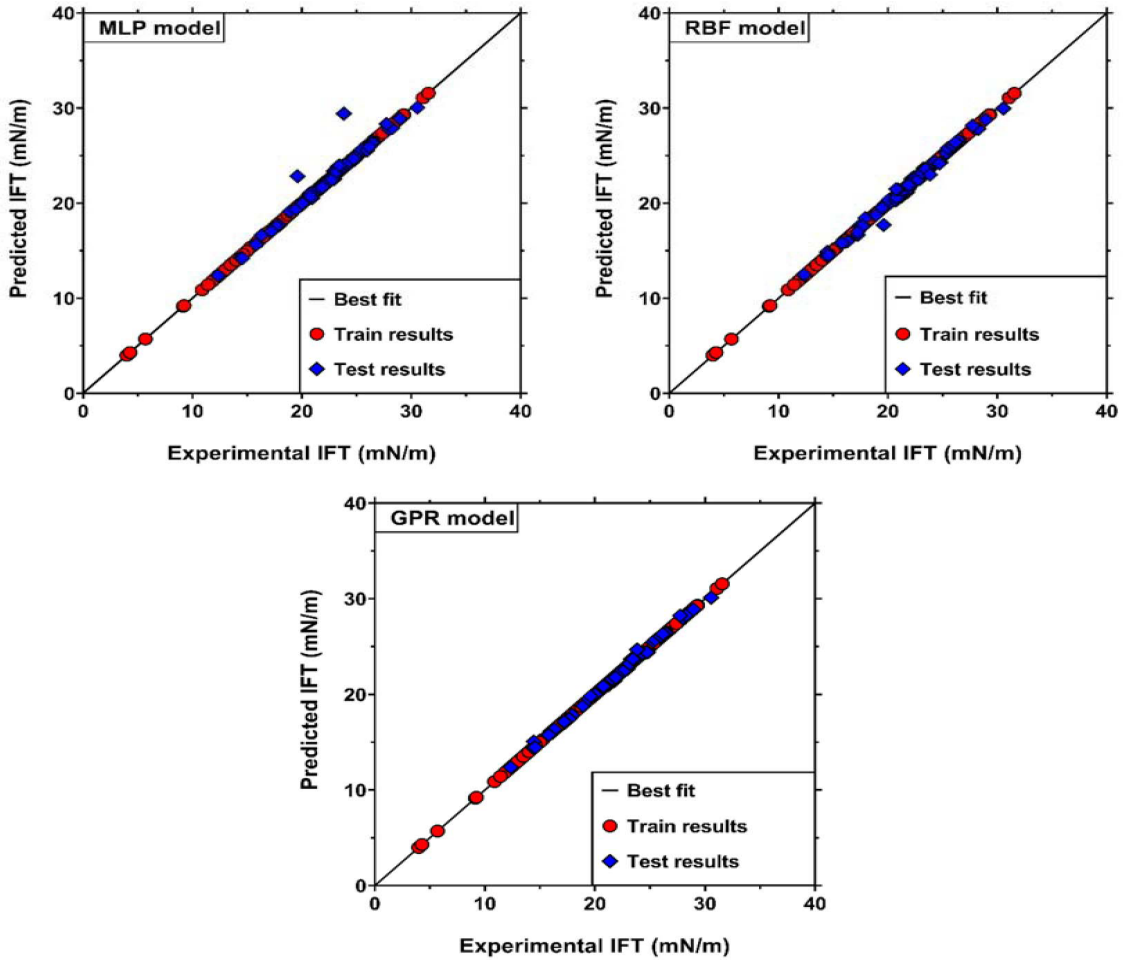

Fig. 7 The cross plots correspond to the novel smart models for estimating the IFT of crude oil-brine systems

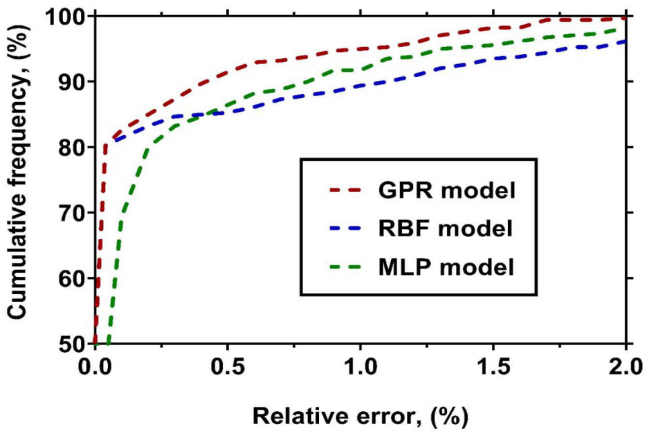

Fig. 8 The cumulative frequency curves correspond to the novel smart models for predicting the IFT of crude oil – brine

To investigate the precision of the smart approaches for estimating the IFT of crude oil-brine systems over diverse ranges of pressure, temperature, brine concentration, and salt molecular weight, the relative errors corresponding to the most reliable model presented in this study, i.e. GPR, have been shown in the contour plots of Fig. 9.

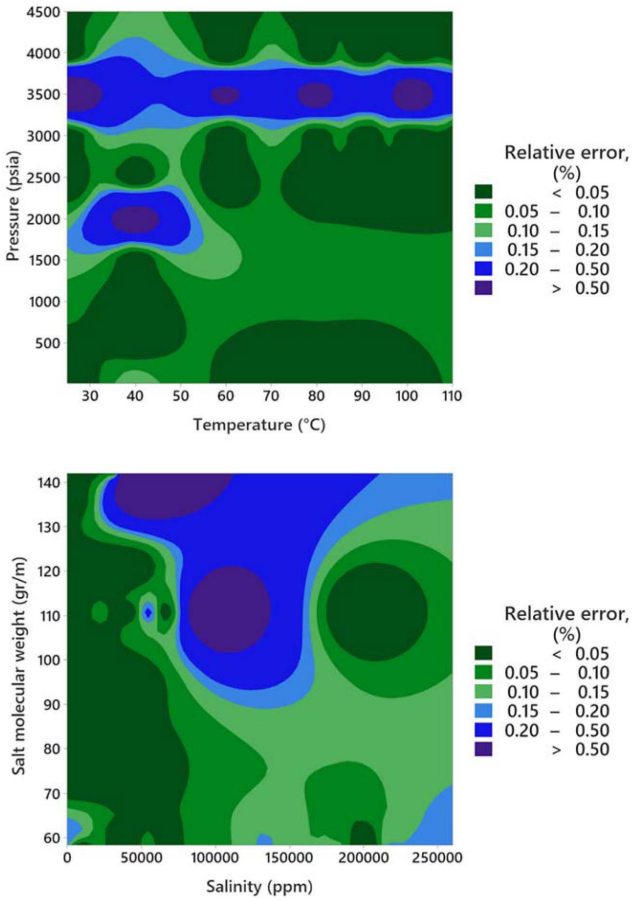

Fig. 9 Distribution of the relative error corresponding to the GPR predictive tool in various ranges of pressure, temperature, brine concentration, and salt molecular weight.

This graphical tool visualizes the distribution of relative error through a color spectrum [77], in which the dark green and purple colors refer to the best and worst estimations, respectively. As it is clear, the dominant parts of the surfaces have been enveloped by green colors, which means that the smart model is capable of estimating the crude oil-brine IFT over a broad range of conditions with relative errors mostly less than 0.15%. On the other hand, there are some blue portions with small and scattered purple shadings, which are predominantly concentrated around P=3500 psia, 100,000<S<150,000 ppm and Mw_s>100 gr/mol. The model may show relative errors higher than 0.15% in the IFT prediction under the foregoing conditions. However, the results obtained based on the cumulative frequency analysis demonstrated that the relative error of the GPR model rarely exceeds 2%. Accordingly, it can be claimed that this predictive tool applies to a wide range of engineering applications with a high level of confidence.

Detection of Outliers

The outlying samples are regarded as some unwilling observations with great divergence from the rest of the data, which may influence the reliability of data-driven models. These data points mostly appear due to human error, uncertainty of measurement devices, complexity of evaluated systems, etc. Thereupon, it is indispensable to explore the established models from the perspective of the existence of doubtful data. The leverage method is a capable technique that identifies the foregoing samples based on William's plot. To implement this approach, the values of standardized residual (SR) and hat values (h) [78,79] should be determined for all analyzed data. According to William's plot, the points situated beyond the h_i<H* and -3<SR<3 domains are recognized as outliers. It should be explained that the warning leverage value, H* can be calculated as follows,

$$H^* = \frac{3(M+1)}{N} \quad (20)$$

where M refers to the number of input variables included in the model, and N denotes the total amount of data. In this study, the smart approaches, which require 7 input factors to determine the IFT of crude oil-brine systems, were established and tested based on 339 data points. Accordingly, the corresponding value of H* is 0.0708. Fig. 10 sketches William's plot corresponding to the most capable IFT model presented in this study, i.e., GPR. The dominant part of the samples lies within the valid limit, confirming the reliability of the collected databank and the proposed model. Meanwhile, only 10 out of 339 data points are recognized as the suspected observations, which are insignificant to affect the capability of the presented models. Hereby, it can be concluded that the smart predictive tools developed in this study have been designed based on credible data points, and they can be confidently used to determine the crude oil-brine IFT.

Capabilities of the proposed models

Description of the physical variations of IFT

The ability to describe physical behaviors is another standard that should be met by a desirable predictive method. In this section, several trend analyses are undertaken to highlight the high capability of the GPR model in predicting the variations of IFT with operational parameters. Indeed, the influences of pressure, temperature, and brine concentration on the IFT of crude oil-brine systems are investigated based on the outcomes of the aforementioned model.

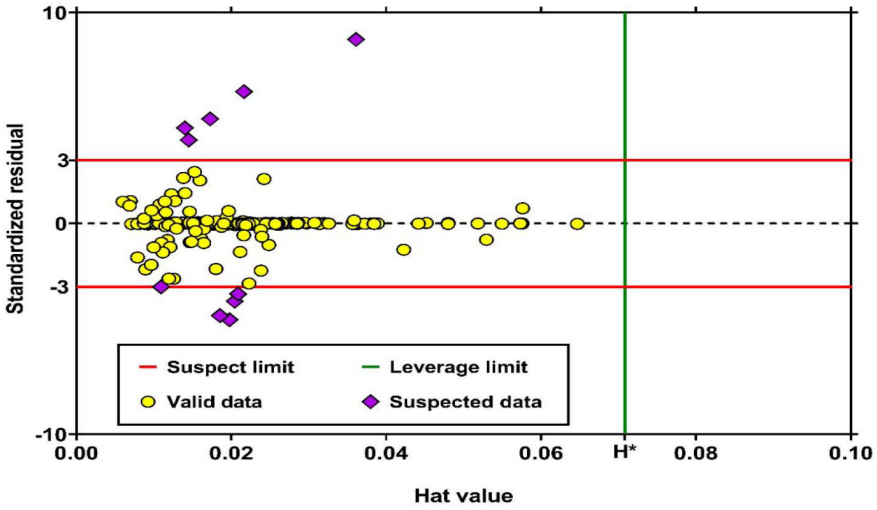

Fig. 10 William's plot of the IFT model designed based on the GPR approach.

Furthermore, the influences of pressure and temperature on the IFT of an asphaltenic crude oil sample blended with an aqueous solution containing 50,000 ppm NaCl are illustrated in Fig. 11. At first glance, it can be found that the IFT of the blend is dramatically reduced with an increase in temperature. This observation can be justified by the growth of total entropy, arising from the increase in molecule mobility at the oil-brine interface, which subsequently declines both Gibbs free energy and IFT [4,42]. On the other hand, the crude oil-brine IFT experiences an ascending trend with an increase in pressure. The preceding change in pressure brings the molecules closer together, and enhances the intermolecular forces, leading to higher IFT values. As it is evident, the GPR predictive method follows the same physical behaviors, and its outcomes are fully consistent with the actual data.

The role of the brine concentration in the variations of the crude oil-brine IFT has been described in Fig. 12. As can be observed, the results indicate the rise of IFT with an increase in salinity under constant pressure and temperature conditions. This behavior can be explained by referring to the Gibbs equation [80],

$$d\gamma = -RT\sum \Gamma_i dLN(a_i) \quad (21)$$

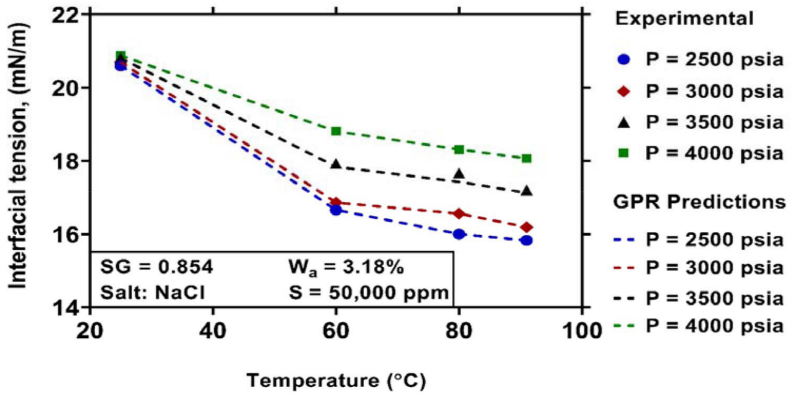

Fig. 11 The variations of the crude oil–brine IFT with pressure and temperature according to experimental data and the outcomes of the GPR model.

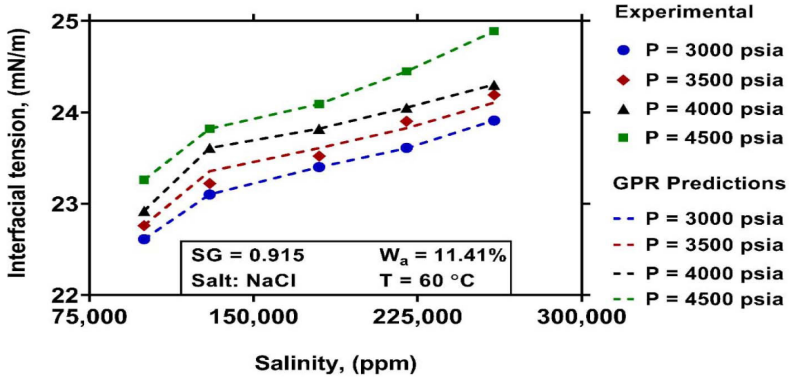

Fig. 12 The variations of the crude oil – brine IFT with salinity according to experimental data and the outcomes of the GPR model.

where Γ_i stands for the surface excess concentration, and α_i is the symbol of chemical activity. Dissolution of salt in water forms hydrogen bonds between salt ions and water molecules. While, the foregoing bonds are not observed at the oil-water interface, and this gives the salt molecules opportunity to transfer from the interface to the bulk of saline water. Thereby, the surface excess concentration of salt tends to a negative value, and the IFT is increased. The values predicted by the proposed model appropriately describe the foregoing physical behaviors, and agree well with the experimental data.

Description of the Role of Various Salts in the IFT Reduction

Fig. 13 compares the best performance of various salts in the IFT reduction, according to the data gathered from Lashkarbolooki et al. [41] and the outcome of the GPR model. This figure reveals that the highest ability in the IFT reduction can be attributed to the salts consisting of Cl^- anion bonded to divalent cations, such as Ca^{+2} and Mg^{+2}. The reaction of the mentioned salts with organic substances included in natural surfactants (resin and asphaltene) produces some complex ions, which are easily dissolved in the water phase. This phenomenon, which is well-known as the salting-in effect leads to a further reduction in the crude oil–brine IFT [81,82]. The results also indicate that the performances of salts declined by replacing Cl^- anion withSO_4^{-2}. This stems from the fact that SO_4^{-2} has lower synergism with the natural surfactants existing in crude oil to reduce the IFT. Additionally, it can be found that the weakest performance in the IFT belongs to the monovalent salts. This can be justified by the low capability of the foregoing salts to boost the migration of natural surfactant molecules from the bulk phase to the interface. As it is evident, the GPR model exactly predicts the performance of all analyzed salts, and this is another testimony concerning its wide applicability.

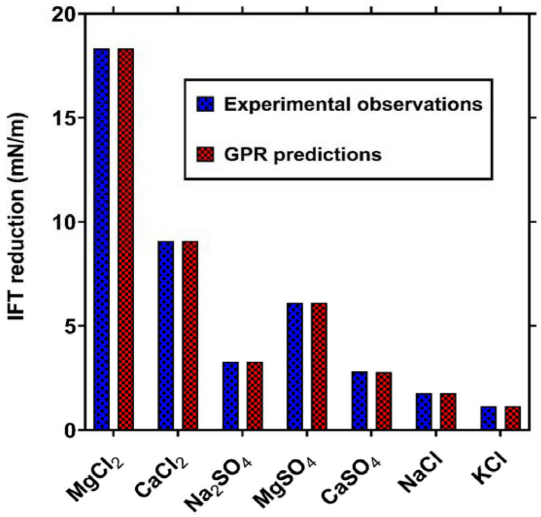

Fig. 13 The role of various salts in the IFT reduction based on experimental data and the outcomes of the GPR model.

Sensitivity Analysis

The current section presents a sensitivity analysis based on the GPR model to determine the order of significance of input variables in controlling the crude oil-brine IFT. Moreover, the relevance of seven input variables to the outcomes of the GPR model is illustrated in Fig. 14. The figure indicates that brine concentration, S, plays the most important role in determining the IFT of crude oil-brine systems, and Mw_g, P, Mw_s, T, and SG are ranked second to sixth, respectively in terms of significance. Eventually, W_a is the factor with the lowest correlation with IFT. The foregoing results are fully consistent with the findings of the analysis carried out in "Determining the input variables of the models" section based on the experimental data.

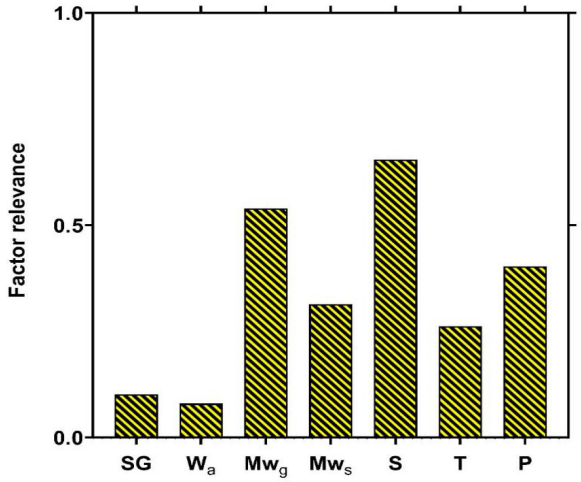

Fig. 14 relevance of seven input factors to the IFT values predicted by the GPR model

Conclusions

This study dealt with the estimation of the IFT between asphaltenic crude oil and brines over a broad range of operating conditions. A widespread set of IFT data, consisting of 339 samples was collected from the literature to achieve this purpose. A comprehensive modeling phase was performed by employing the smart soft-computing approaches of MLP, RBF, and GPR. The main findings of this research can be expressed as follows,

• Defining seven parameters, including P, T, S, W_a, SG, Mw_g and Mw_s as the model's input variables led to much more accurate predictions for the crude oil-brine IFT. This fact was also confirmed by the analysis performed based on Spearman's rank coefficient.

• All proposed models were accurate and capable tools for the scope of the current study, with AARE values between 0.67% and 1.45%, and R^2 values higher than 99.60%.

• The correctness and reliability of the proposed models were evaluated based on a set of graphical representations, and the results demonstrated the obvious superiority of the GPR method. The aforementioned model estimated the crude oil-brine IFT over a broad range of operating conditions with relative errors below 0.10%.

• The GPR model was a desirable computational approach to predict the physical variations of IFT. Moreover, it was applicable to describe the performances of different salts in the IFT reduction.

• An analysis undertaken through the leverage method indicated that the IFT databank analyzed in this study is highly credible since less than 3% of all data were recognized as doubtful observations.

• According to the sensitivity analysis based on the GPR

model, brine concentration, S, is the most effective input variable on the model performance, and Mw_g, P, Mw_s, T, SG, and W_a are ranked second to seventh in terms of significance, respectively.

Overall, the smart models presented in this study are precise, reliable, and comprehensive tools to estimate the asphaltenic crude oil-brine IFT. Thereupon, they in turn contribute to the optimal design of the EOR processes.

Data Availability Statement

The data that support the findings of this study are available from the corresponding author upon reasonable request.

Nomenclatures

AARE: Average absolute relative error, %
E_i: Relative error from the actual value
Mw_g: Equivalent molecular weight of dissolved gases, g/mol
Mw_s: Molecular weight of salt, g/mol
N: Number of experimental data
P: Pressure, Pa
R: Universal gas constant, m^3.Pa/mol.K
R^2: Coefficient of determination, %
RRMSE: Relative root mean square error, %
S: Salinity, ppm
SD: Standard deviation, %
SG: Specific gravity
T: Temperature, (°C)
W_a: Percentage of the asphaltenes in crude oil, %

Greek

α: Chemical activity
Γ: Surface excess concentration
γ: Interfacial tension, (mN/m)

Subscripts

exp: Experimental
pre: Predicted by Model

Abbreviations

GPR: Gaussian process regression
IFT: Interfacial tension
MLP: Multilayer perceptron
RBF: Radial basis function

References

1. Niroomand-Toomaj, E., Etemadi, A., & Shokrollahi, A. (2017). Radial basis function modeling approach to prognosticate the interfacial tension CO_2/Aquifer Brine. Journal of Molecular Liquids, 238, 540-544. doi.org/10.1016/j.molliq.2017.04.135.
2. Jiao, F., Al Ghafri, S. Z., Seneviratne, K. N., Akhfash, M., Hughes, T. J., Johns, M. L., & May, E. F. (2022). Interfacial tension measurements of methane plus propane binary and methane plus propane plus n-heptane ternary mixtures at low temperatures. Journal of Chemical Thermodynamics, 171. doi.org/10.1016/j.jct.2022.106786.
3. Zhang, C., & Wang, M. (2023). CO_2/brine interfacial tension for geological CO_2 storage: A systematic review. Journal of Petroleum Science and Engineering, 220, 111154. doi.org/10.1016/j.petrol.2022.111154.
4. Barati-Harooni, A., Soleymanzadeh, A., Tatar, A., Najafi-Marghmaleki, A., Samadi, S. J., Yari, A., Roushani B., & Mohammadi, A. H. (2016). Experimental and modeling studies on the effects of temperature, pressure and brine salinity on interfacial tension in live oil-brine systems. Journal of Molecular Liquids, 219, 985-993. doi.org/10.1016/j.molliq.2016.04.013.
5. Hosseinzadeh Dehaghani, Y., Assareh, M., & Feyzi, F. (2022). Simultaneous prediction of equilibrium, interfacial, and transport properties of CO_2-brine systems using molecular dynamics simulation: applications to CO_2 storage. Industrial & Engineering Chemistry Research, 61(41), 15390-15406. doi.org/10.1021/acs.iecr.2c02249.
6. Lim, S. S. S., Elochukwu, H., Nandong, J., Bennour, Z., & Hamid, M. A. (2023). A review on the mechanisms of low salinity water/surfactant/nanoparticles and the potential synergistic application for c-EOR. Petroleum Research, 8(3), 324-337. doi.org/10.1016/j.ptlrs.2023.02.001.
7. Sheng J. J. (2020) EOR mechanisms of wettability alteration and its comparison with IFT, Enhanc. Oil Recover. Shale Tight Reserv. 213–278. doi.org/10.1016/b978-0-12-815905-7.00009-8.
8. Safaei-Farouji, M., Thanh, H. V., Dashtgoli, D. S., Yasin, Q., Radwan, A. E., Ashraf, U., & Lee, K. K. (2022). Application of robust intelligent schemes for accurate modelling interfacial tension of CO_2 brine systems: Implications for structural CO_2 trapping. Fuel, 319, 123821. doi.org/10.1016/j.fuel.2022.123821.
9. Mokhtari, R., Ayatollahi, S., & Fatemi, M. (2019). Experimental investigation of the influence of fluid-fluid interactions on oil recovery during low salinity water flooding. Journal of Petroleum Science and Engineering, 182, 106194. doi.org/10.1016/j.petrol.2019.106194.
10. eng X., Tariq Z., Murtaza M., Patil S., Mahmoud M., Kamal M.S. (2021). Relative contribution of wettability Alteration and interfacial tension reduction in EOR: A critical review. Journal of Molecular Liquids, 325, 115175. doi.org/10.1016/j.molliq.2020.115175.
11. Su, C. H., & Chen, L. J. (2016). Phase behavior and interfacial tensions in the ternary systems water+ dodecane+ propylene glycol n-propyl ether and water+ tetradecane+ propylene glycol n-propyl ether. Journal of the Taiwan Institute of Chemical Engineers, 68, 74-79. doi.org/10.1016/j.jtice.2016.09.019.
12. Lashkarbolooki, M., Riazi, M., & Ayatollahi, S. (2017). Effect of CO_2 and natural surfactant of crude oil on the dynamic interfacial tensions during carbonated water flooding: experimental and modeling investigation. Journal of Petroleum Science and Engineering, 159, 58-67. doi.org/10.1016/j.petrol.2017.09.023.
13. Shang, Q., Xia, S., Cui, G., Tang, B., & Ma, P. (2018). Experiment and correlation of the equilibrium interfacial tension for paraffin+ CO_2 modified with ethanol. The Journal of Chemical Thermodynamics, 116, 206-212. doi.org/10.1016/j.jct.2017.08.031.
14. Zhang, K., Georgiadis, A., & Trusler, J. M. (2022). Measurements and interpretation of crude Oil-Water/

Brine dynamic interfacial tension at subsurface representative conditions. Fuel, 315, 123266. doi.org/10.1016/j.fuel.2022.123266.

15. Zandahvifard, M. J., Elhambakhsh, A., Ghasemi, M. N., Esmaeilzadeh, F., Parsaei, R., Keshavarz, P., & Wang, X. (2021). Effect of modified Fe_3O_4 magnetic NPs on the absorption capacity of CO_2 in water, wettability alteration of carbonate rock surface, and water–oil interfacial tension for oilfield applications. Industrial & Engineering Chemistry Research, 60(8), 3421-3434. doi.org/10.1021/acs.iecr.0c04857.
16. Choudhary, N., Anwari Che Ruslan, M. F., Narayanan Nair, A. K., Qiao, R., & Sun, S. (2021). Bulk and interfacial properties of the decane+ brine system in the presence of carbon dioxide, methane, and their mixture. Industrial & Engineering Chemistry Research, 60(30), 11525-11534. doi.org/10.1021/acs.iecr.1c01607.
17. Liu, J., Liu, S., Zhong, L., Yuan, S., Wang, Q., & Wei, C. (2023). Study on the emulsification characteristics of heavy oil during chemical flooding. Physics of Fluids, 35(5). doi.org/10.1063/5.0152109.
18. Farhadi, H., Ayatollahi, S., & Fatemi, M. (2021). The effect of brine salinity and oil components on dynamic IFT behavior of oil-brine during low salinity water flooding: Diffusion coefficient, EDL establishment time, and IFT reduction rate. Journal of Petroleum Science and Engineering, 196, 107862. doi.org/10.1016/j.petrol.2020.107862.
19. Behvandi, R., & Mirzaie, M. (2022). A novel correlation for modeling interfacial tension in binary mixtures of CH, CO, and N^+ normal alkanes systems: Application to gas injection EOR process. Fuel, 325, 124622. doi.org/10.1016/j.fuel.2022.124622.
20. Talebian, S. H., Fahimifar, A., & Heidari, A. (2021). Review of enhanced oil recovery decision making in complex carbonate reservoirs: Fluid flow and geomechanics mechanisms. Journal of Computational Applied Mechanics, 52(2), 350-365. doi.org/10.22059/jcamech.2021.318511.596.
21. Negi, G. S., Sircar, A., & Pandian, S. (2023). Engineering the rheology and IFT behavior of mixed formulations of anionic and non-ionic surfactants with added silica nanoparticles. Materials Today: Proceedings, 77, 223-233. doi.org/10.1016/j.matpr.2022.11.266.
22. Lins, I. E., Santana, G. P., Costa, G. M., & de Melo, S. A. V. (2022). New correlations for interfacial tension of CO2-water-electrolyte systems at high pressure. Fluid Phase Equilibria, 555, 113354. doi.org/10.1016/j.fluid.2021.113354.
23. Najimi, S., Nowrouzi, I., Manshad, A. K., Farsangi, M. H., Hezave, A. Z., Ali, J. A., Keshavarz A., & Mohammadi, A. H. (2019). Investigating the effect of [C 8Py][Cl] and [C18Py][Cl] ionic liquids on the water/oil interfacial tension by considering Taguchi method. Journal of Petroleum Exploration and Production Technology, 9, 2933-2941. doi.org/10.1007/s13202-019-0688-8.
24. Jerauld, G. R., & Kazemi, A. (2022). An improved simple correlation for accurate estimation of CO_2-Brine interfacial tension at reservoir conditions. Journal of Petroleum Science and Engineering, 208, 109537. doi.org/10.1016/j.petrol.2021.109537.
25. Li, N., Zhang, C., Ma, Q., Sun, Z., Chen, Y., Jia, S., Chen G., Sun C., & Yang, L. (2019). Measurements and modeling of interfacial tension for (CO_2+ n-alkyl benzene) binary mixtures. The Journal of Supercritical Fluids, 154, 104625. doi.org/10.1016/j.supflu.2019.104625.
26. Li, N., Zhang, C., Ma, Q., Sun, Z., Chen, Y., Jia, S., Chen G., Sun C. & Yang, L. (2019). Measurements and modeling of interfacial tension for (CO_2+ n-alkyl benzene) binary mixtures. The Journal of Supercritical Fluids, 154, 104625. doi.org/10.1016/j.supflu.2019.104625.
27. Asadzadeh, N., Ahmadlouydarab, M., & Haddad, A. S. (2023). Effects of temperature and nanofluid type on the oil recovery from a vertical porous media in antigravity fluid injection. Chemical Engineering Research and Design, 193, 394-408. doi.org/10.1016/j.cherd.2023.03.046.
28. Song, Y., Song, Z., Guo, J., Feng, D., & Chang, X. (2021). Phase behavior and miscibility of CO_2–hydrocarbon mixtures in shale nanopores. Industrial & Engineering Chemistry Research, 60(14), 5300-5309. doi.org/10.1021/acs.iecr.1c00717.
29. Tang, X., Li, Y., Cao, J., Liu, Z., Chen, X., Liu, L., Zhang Y. & Li, Q. (2023). Adaptability and enhanced oil recovery performance of surfactant–polymer flooding in inverted seven-spot well pattern. Physics of Fluids, 35(5). doi.org/10.1063/5.0147806.
30. Liu, X., Kang, Y., Yan, L., Tian, J., Li, J., & You, L. (2022). Implication of interfacial tension reduction and wettability alteration by surfactant on enhanced oil recovery in tight oil reservoirs. Energy Reports, 8, 13672-13681. doi.org/10.1016/j.egyr.2022.10.052.
31. Tu, J., & Sheng, J. J. (2020). Experimental and numerical study of surfactant solution spontaneous imbibition in shale oil reservoirs. Journal of the Taiwan Institute of Chemical Engineers, 106, 169-182. doi.org/10.1016/j.jtice.2019.11.003.
32. Mohamed, A. I., Khishvand, M., & Piri, M. (2023). Entrapment and mobilization dynamics during the flow of viscoelastic fluids in natural porous media: A micro-scale experimental investigation. Physics of Fluids, 35(4). doi.org/10.1063/5.0139401.
33. Talebian, S. H., Masoudi, R., Tan, I. M., & Zitha, P. L. J. (2014). Foam assisted CO2-EOR: A review of concept, challenges, and future prospects. Journal of Petroleum Science and Engineering, 120, 202-215. doi.org/10.1016/j.petrol.2014.05.013.
34. Garrido, J. M., Cifuentes, L., Cartes, M., Segura, H., & Mejía, A. (2014). High-pressure interfacial tensions for nitrogen+ ethanol, or hexane or 2-methoxy-2-methylbutane: A comparison between experimental tensiometry and Monte Carlo simulations. The Journal of Supercritical Fluids, 89, 78-88. doi.org/10.1016/j.supflu.2014.02.012.
35. Tsuzuki, R., Tanaka, R., Ban, T., & Nagatsu, Y. (2019). Deviation from capillary number scaling of nonlinear viscous fingering formed by the injection of Newtonian

surfactant solution. Physics of Fluids, 31(4). doi.org/10.1063/1.5090827.
36. Gandomkar, A., Sheykhneshin, M. G., Nasriani, H. R., Yazdkhasti, P., & Safavi, M. S. (2022). Enhanced oil recovery through synergy of the interfacial mechanisms by low salinity water alternating carbon dioxide injection. Chemical Engineering Research and Design, 188, 462-472. doi.org/10.1016/j.cherd.2022.09.053.
37. Zhao, H., Kang, W., Yang, H., Zhang, H., Zhu, T., Wang, F., Li, X., Zhou, B., Sarsenbekuly, B., Aidarova, S. and Ibrashev, K., (2020). Imbibition enhancing oil recovery mechanism of the two surfactants. Physics of Fluids, 32(4). doi.org/10.1063/5.0005106.
38. Bollineni, P. K., Dordzie, G., Olayiwola, S. O., & Dejam, M. (2021). An experimental investigation of the viscosity behavior of solutions of nanoparticles, surfactants, and electrolytes. Physics of Fluids, 33(2). doi.org/10.1063/5.0038002.
39. Narayanan Nair, A. K., Che Ruslan, M. F. A., Cui, R., & Sun, S. (2022). An overview of the oil+ brine two-phase system in the presence of carbon dioxide, methane, and their mixture. Industrial & Engineering Chemistry Research, 61(49), 17766-17782. doi.org/10.1021/acs.iecr.2c03089.
40. Lashkarbolooki, M., & Ayatollahi, S. (2018). The effects of pH, acidity, asphaltene and resin fraction on crude oil/water interfacial tension. Journal of Petroleum Science and Engineering, 162, 341-347. doi.org/10.1016/j.petrol.2017.12.061.
41. Lashkarbolooki, M., Ayatollahi, S., & Riazi, M. (2014). The impacts of aqueous ions on interfacial tension and wettability of an asphaltenic–acidic crude oil reservoir during smart water injection. Journal of Chemical & Engineering Data, 59(11), 3624-3634. doi.org/10.1021/je500730e.
42. Moeini, F., Hemmati-Sarapardeh, A., Ghazanfari, M. H., Masihi, M., & Ayatollahi, S. (2014). Toward mechanistic understanding of heavy crude oil/brine interfacial tension: The roles of salinity, temperature and pressure. Fluid phase equilibria, 375, 191-200. doi.org/10.1016/j.fluid.2014.04.017.
43. Soleymanzadeh, A., Rahmati, A., Yousefi, M., & Roshani, B. (2021). Theoretical and experimental investigation of effect of salinity and asphaltene on IFT of brine and live oil samples. Journal of Petroleum Exploration and Production, 11, 769-781. doi.org/10.1007/s13202-020-01020-1.
44. Abdi, A., Ranjbar, B., Kazemzadeh, Y., Aram, F., & Riazi, M. (2024). Investigating the mechanism of interfacial tension reduction through the combination of low-salinity water and bacteria. Scientific Reports, 14(1), 11408. doi.org/10.1038/s41598-024-62255-0.
45. Ali, S. I., Lalji, S. M., Hashmi, S., Awan, Z., Iqbal, A., & Al-Ammar, E. A. (2024). Risk quantification and ranking of oil fields and wells facing asphaltene deposition problem using fuzzy TOPSIS coupled with AHP. Ain Shams Engineering Journal, 15(1), 102289. doi.org/10.1016/j.asej.2023.102289.
46. Fakher, S., Ahdaya, M., Elturki, M., & Imqam, A. (2020). Critical review of asphaltene properties and factors impacting its stability in crude oil. Journal of Petroleum Exploration and Production Technology, 10, 1183-1200. doi.org/10.1007/s13202-019-00811-5.
47. Mehrjoo, H., Riazi, M., Amar, M. N., & Hemmati-Sarapardeh, A. (2020). Modeling interfacial tension of methane-brine systems at high pressure and high salinity conditions. Journal of the Taiwan Institute of Chemical Engineers, 114, 125-141. doi.org/10.1016/j.jtice.2020.09.014.
48. Amar, M. N., Shateri, M., Hemmati-Sarapardeh, A., & Alamatsaz, A. (2019). Modeling oil-brine interfacial tension at high pressure and high salinity conditions. Journal of Petroleum Science and Engineering, 183, 106413. doi.org/10.1016/j.petrol.2019.106413.
49. Behnamnia, M., Monfared, A. D., & Sarmadivaleh, M. (2022). Hybrid artificial intelligence paradigms for modeling of water-gas (pure/mixture) interfacial tension. Journal of Natural Gas Science and Engineering, 108, 104812. doi.org/10.1016/j.jngse.2022.104812.
50. Amar, M. N. (2021). Towards improved genetic programming based-correlations for predicting the interfacial tension of the systems pure/impure CO2-brine. Journal of the Taiwan Institute of Chemical Engineers, 127, 186-196. doi.org/10.1016/j.jtice.2021.08.010.
51. Cao, Y., Du, J., Bai, Y., Ghadiri, M., & Mohammadinia, S. (2021). Towards estimating surface tension of biodiesels: Application to thermodynamic and intelligent modeling. Fuel, 283, 118797. doi.org/10.1016/j.fuel.2020.118797.
52. Deng, J., Zhang, Y., & Jia, G. (2023). Surface tension of binary and ternary mixtures mapping with ASP and UNIFAC models based on machine learning. Physics of Fluids, 35(6). doi.org/10.1063/5.0152893.
53. Sulaiman, M., & Khan, N. A. (2023). Predictive modeling of oil and water saturation during secondary recovery with supervised learning. Physics of Fluids, 35(6). doi.org/10.1063/5.0152071.
54. Ayatollahi, S., Hemmati-Sarapardeh, A., Roham, M., & Hajirezaie, S. (2016). A rigorous approach for determining interfacial tension and minimum miscibility pressure in paraffin-CO_2 systems: Application to gas injection processes. Journal of the Taiwan Institute of Chemical Engineers, 63, 107-115. doi.org/10.1016/j.jtice.2016.02.013.
55. Rowane, A. J., Gupta, A., Gavaises, M., & McHugh, M. A. (2020). Experimental and modeling investigations of the interfacial tension of three different diesel+ nitrogen mixtures at high pressures and temperatures. Fuel, 280, 118543. doi.org/10.1016/j.fuel.2020.118543.
56. Cumicheo, C., Cartes, M., Müller, E. A., & Mejía, A. (2018). Experimental measurements and theoretical modeling of high-pressure mass densities and interfacial tensions of carbon dioxide+ n-heptane+ toluene and its carbon dioxide binary systems. Fuel, 228, 92-102. doi.org/10.1016/j.fuel.2018.04.057.
57. Danzer, A., & Enders, S. (2018). Comparison of two modelling approaches for the interfacial tension of binary aqueous mixtures. Journal of Molecular Liquids, 266, 309-320. doi.org/10.1016/j.molliq.2018.06.061.
58. Rashid S., Harimi B. & Hamidpour E. (2017). Prediction of CO2-Brine interfacial tension using a

rigorous approach. Journal of Natural Gas Science and Engineering, 45, 108-117. doi.org/10.1016/j.jngse.2017.05.002.

59. Mirzaie, M., & Tatar, A. (2020). Modeling of interfacial tension in binary mixtures of CH4, CO_2, and N2-alkanes using gene expression programming and equation of state. Journal of Molecular Liquids, 320, 114454. doi.org/10.1016/j.molliq.2020.114454.
60. Ameli, F., Hemmati-Sarapardeh, A., Tatar, A., Zanganeh, A., & Ayatollahi, S. (2019). Modeling interfacial tension of normal alkane-supercritical CO2 systems: Application to gas injection processes. Fuel, 253, 1436-1445. doi.org/10.1016/j.fuel.2019.05.078.
61. Abooali, D., Sobati, M. A., Shahhosseini, S., & Assareh, M. (2019). A new empirical model for estimation of crude oil/brine interfacial tension using genetic programming approach. Journal of Petroleum Science and Engineering, 173, 187-196. doi.org/10.1016/j.petrol.2018.09.073.
62. Chowdhury, S., Shrivastava, S., Kakati, A., & Sangwai, J. S. (2022). Comprehensive review on the role of surfactants in the chemical enhanced oil recovery process. Industrial & Engineering Chemistry Research, 61(1), 21-64. doi.org/10.1021/acs.iecr.1c03301.
63. Hosseini, S. H., Moradkhani, M. A., Rasteh, M., & Rahimi, M. (2021). New smart models for minimum fluidization velocity forecasting in the tapered fluidized beds based on particle size distribution. Industrial & Engineering Chemistry Research, 60(42), 15289-15300. doi.org/10.1021/acs.iecr.1c02682.
64. Moradkhani, M. A., Hosseini, S. H., Mansouri, M., Zad, H. O., Karami, M., & Ahmadi, G. (2022). New general models for condensation heat transfer coefficient of carbon dioxide in smooth tubes by intelligent and least square fitting approaches. Journal of Cleaner Production, 330, 129762. doi.org/10.1016/j.jclepro.2021.129762.
65. Moradkhani, M. A., Hosseini, S. H., Karami, M., Olazar, M., & Saldarriaga, J. F. (2023). Applying conventional and intelligent approaches to model the minimum spouting velocity of vegetable biomasses in conical spouted beds. Powder Technology, 418, 118300. doi.org/10.1016/j.powtec.2023.118300.
66. Moradkhani, M. A., Hosseini, S. H., Valizadeh, M., & Mengjie, S. O. N. G. (2021). Machine learning based models to predict frost characteristics on cryogenic surfaces under forced convection conditions. International Communications in Heat and Mass Transfer, 129, 105667. doi.org/10.1016/j.icheatmasstransfer.2021.105667.
67. Hosseini, S. H., Rezaei, M. J., Bag-Mohammadi, M., Karami, M., Moradkhani, M. A., Panahi, M., & Olazar, M. (2019). Estimation of the minimum spouting velocity in shallow spouted beds by intelligent approaches: Study of fine and coarse particles. Powder Technology, 354, 456-465. doi.org/10.1016/j.powtec.2019.06.025.
68. Liu, W., Qi, H., Shi, H., Yu, C., & Li, X. (2023). Helical model based on artificial neural network for large eddy simulation of compressible wall-bounded turbulent flows. Physics of Fluids, 35(4). doi.org/10.1063/5.0137607.
69. Moradkhani, M. A., Hosseini, S. H., & Ranjbar, K. (2023). Universal intelligent models for liquid density of CO_2+ hydrocarbon mixtures. Fuel, 334, 126642. doi.org/10.1016/j.fuel.2022.126642.
70. Alipanahi, E., Moradkhani, M. A., Zolfaghari, A., & Bayati, B. (2023). Robust intelligent approaches to predict the CO_2 frosting temperature in natural gas mixtures under cryogenic conditions. International Journal of Refrigeration, 154, 281-289. doi.org/10.1016/j.ijrefrig.2022.11.018.
71. Moradkhani, M. A., Hosseini, S. H., Shangwen, L., & Mengjie, S. (2022). Intelligent computing approaches to forecast thickness and surface roughness of frost layer on horizontal plates under natural convection. Applied Thermal Engineering, 217, 119258. doi.org/10.1016/j.applthermaleng.2022.119258.
72. Moradi, M., Moradkhani, M. A., Hosseini, S. H., & Olazar, M. (2023). Intelligent modeling of photocatalytically reactive yellow 84 azo dye removal from aqueous solutions by ZnO-light expanded clay aggregate nanoparticles. International Journal of Environmental Science and Technology, 20(3), 3009-3022. doi.org/10.1007/s13762-022-04728-1.
73. Moradkhani, M. A., Hosseini, S. H., Ranjbar, K., & Moradi, M. (2023). Intelligent modeling of hydrogen sulfide solubility in various types of single and multicomponent solvents. Scientific Reports, 13(1), 3777. doi.org/10.1038/s41598-023-30777-8.
74. Xue, H., Wang, C., Jiang, L., Wang, H., Lv, Z., Huang, J., & Xiao, W. (2022). Asphaltene precipitation trend and controlling its deposition mechanism. Natural Gas Industry B, 9(1), 84-95. doi.org/10.1016/j.ngib.2021.12.001.
75. Bolboaca, S. D., & Jäntschi, L. (2006). Pearson versus Spearman, Kendall's tau correlation analysis on structure-activity relationships of biologic active compounds. Leonardo Journal of Sciences, 5(9), 179-200.
76. Zendehboudi, A., & Li, X. (2017). A robust predictive technique for the pressure drop during condensation in inclined smooth tubes. International Communications in Heat and Mass Transfer, 86, 166-173. doi.org/10.1016/j.icheatmasstransfer.2017.05.030.
77. Mahdaviara, M., Rostami, A., Helalizadeh, A., & Shahbazi, K. (2021). Smart modeling of viscosity of viscoelastic surfactant self-diverting acids. Journal of Petroleum Science and Engineering, 196, 107617. doi.org/10.1016/j.petrol.2020.107617.
78. Mahdaviara, M., Rostami, A., Keivanimehr, F., & Shahbazi, K. (2021). Accurate determination of permeability in carbonate reservoirs using Gaussian Process Regression. Journal of Petroleum Science and Engineering, 196, 107807. doi.org/10.1016/j.petrol.2020.107807.
79. Mahdaviara, M., Amar, M. N., Ostadhassan, M., & Hemmati-Sarapardeh, A. (2022). On the evaluation of the interfacial tension of immiscible binary systems of methane, carbon dioxide, and nitrogen-alkanes using robust data-driven approaches. Alexandria Engineering Journal, 61(12), 11601-11614. doi.org/10.1016/j.aej.2022.04.049.

80. Guggenheim, E. A., & Adam, N. K. (1933). The thermodynamics of adsorption at the surface of solutions. Proceedings of the Royal Society of London. Series A, Containing Papers of a Mathematical and Physical Character, 139(837), 218-236. doi.org/10.1098/rspa.1933.0015.
81. Austad, T. (2013). Water-based EOR in carbonates and sandstones: new chemical understanding of the EOR potential using "smart water". In Enhanced oil recovery Field case studies (pp. 301-335). Gulf Professional Publishing. doi.org/10.1016/B978-0-12-386545-8.00013-0.
82. Qiao, W., Li, J., Zhu, Y., & Cai, H. (2012). Interfacial tension behavior of double long-chain 1, 3, 5-triazine surfactants for enhanced oil recovery. Fuel, 96, 220-225. doi.org/10.1016/j.fuel.2012.01.014.